# Lawrence Berkeley National Laboratory

**Applied Math & Comp Sci**

## Title
Transition in swimming direction in a model self-propelled inertial swimmer

## Permalink
https://escholarship.org/uc/item/9qk8127k

## Journal
Physical Review Fluids, 4(2)

## ISSN
2469-9918

## Authors
Dombrowski, Thomas
Jones, Shannon K
Katsikis, Georgios
et al.

## Publication Date
2019-02-01

## DOI
10.1103/physrevfluids.4.021101

Peer reviewed

# Transition in motility mechanism due to inertia in a model self-propelled two-sphere swimmer

Shannon K. Jones,[1] Amneet Pal Singh Bhalla,[2] Georgios Katsikis,[3] Boyce E. Griffith,[4] and Daphne Klotsa[1, *]

[1]*Department of Applied Physical Sciences, The University of North Carolina at Chapel Hill, Chapel Hill, NC, USA*
[2]*Applied Numerical Algorithms Group, Lawrence Berkeley National Laboratory, Berkeley, CA, USA*
[3]*Koch Institute for Integrative Cancer Research, Massachusetts Institute of Technology, Cambridge, Massachusetts, USA*
[4]*Departments of Mathematics, Applied Physical Sciences, and Biomedical Engineering,*
*The University of North Carolina at Chapel Hill, Chapel Hill, NC, USA*
(Dated: January 15, 2018)

We propose a model reciprocal swimmer composed of two unequal spheres that oscillate with respect to each other, and we use computer modeling to study its motility for $0 \leq Re \leq 150$. We show that our model switches swimming direction from a small-sphere-leading to a large-sphere-leading regime at $Re \approx 30$. Thus, although the relative oscillation of the spheres is the same in all cases, the two flow regimes yield distinct motility mechanisms. The generated flows are qualitatively similar to pullers and pushers in Stokes flows, except that here inertial forces play an important role in the system dynamics. We relate both motility mechanisms to the classical nonlinear phenomenon of steady streaming, suggesting that steady streaming can be an important physical mechanism in swimming at intermediate $Re$. As a step towards classifying swimming at intermediate Reynolds numbers, we introduce the concepts of *steady streaming pullers* and *steady streaming pushers*.

**PACS numbers:** May be entered using the \pacs{#1} command.

Diverse biological motion occurs in fluid environments across a broad range of scales. Examples include active and passive transport at subcellular scales as well as swimming bacteria, tunicates, seahorses, jellyfish, sharks, and whales. [1–3]. Understanding biological motility requires connections between fundamental physics and biology and has many applications, including drug-delivering nanomachines [4, 5] and autonomous underwater vehicles [6–8]. Swimming regimes can be classified by the Reynolds number ($Re$), which characterizes the relative importance of inertial and viscous forces. Although there is a large body of work on motility in Stokes flows ($Re = 0$), in which viscous forces dominate, and at high $Re$, in which inertial forces dominate, less is known about the intermediate regime $Re_{int} \sim 1 – 1000$.

The intermediate $Re$ regime encompasses an enormous diversity of organisms, ranging from larvae (fish, squid, ascidian) and large ciliates, to nematodes, copepods, and jellyfish, that exhibit a variety of motility mechanisms: jet propulsion [9, 10], anguilliform (eel-like) locomotion [11–15], rowing [16, 17], aquatic flapping flight [18], and ciliate beating [19, 20]. Previous work to develop and classify model swimmers has focused on Stokes flows [21, 22], as with the spherical squirmer model of *pushers* and *pullers* [23–30]. The breadth of the motility mechanisms encountered in nature, together with the lack of analytical solutions to the Navier-Stokes equations at $Re_{int}$, has made it difficult to develop a similar classification system in the intermediate regime. Consequently, most prior studies at $Re_{int}$ have focused on the details of specific organisms [9–12, 14–20, 31–33], sometimes treating $Re_{int}$ swimmers under Stokes assumptions for simplicity [13, 34]. The squirmer model was recently extended to include inertia, which is providing useful in-

sights [35–38]. However, there is still no quantitative classification of model swimmers at $Re_{int}$. It is important to develop general models that make few *a priori* assumptions, so that the underlying physical mechanisms and characteristics of these swimmers can be identified and understood. Only then can we make progress in better understanding the biology and designing artificial swimmers.

In this paper we propose a *spherobot* model reciprocal swimmer that is composed of two unequal spheres that oscillate with respect to each other (Fig. 1(a)), and computationally studied its motility for $0.001 \leq Re \leq 150$ as well as in Stokes flow. For $Re = 0$, the spherobot cannot swim because of Purcell's scallop theorem [39]; its reciprocal stroke does not break time-reversible symmetry. For $Re \geq 0.001$ the spherobot begins swimming with the small sphere leading, and then switches direction at $Re \approx 30$ to swim with the large sphere leading. We analyzed the flow fields for each regime of swimming direction and showed that they qualitatively correspond to the flow fields of Stokesian pullers and pushers, respectively. Unlike Stokesian swimmers, however, the spherobot uses steady streaming to swim, which is characteristic of oscillatory flows at $Re_{int}$ [40, 41]. We suggest that steady streaming can be an important physical mechanism present more generally in motility at $Re_{int}$ [42–45].

The spherobot is composed of two unequal sized spheres, which are coupled to one another by prescribing the distance between their centers $d(t) = d_0 + A_r \sin(2\pi f t)$, in which $d_0$ is the distance between the sphere centers in the middle of the cycle, $A_r = 0.5(d_{max} - d_{min})$ is the relative amplitude of the spherobot, and $f$ is the frequency of oscillation (Fig. 1(a)). To model this computationally, we tethered the two spheres using
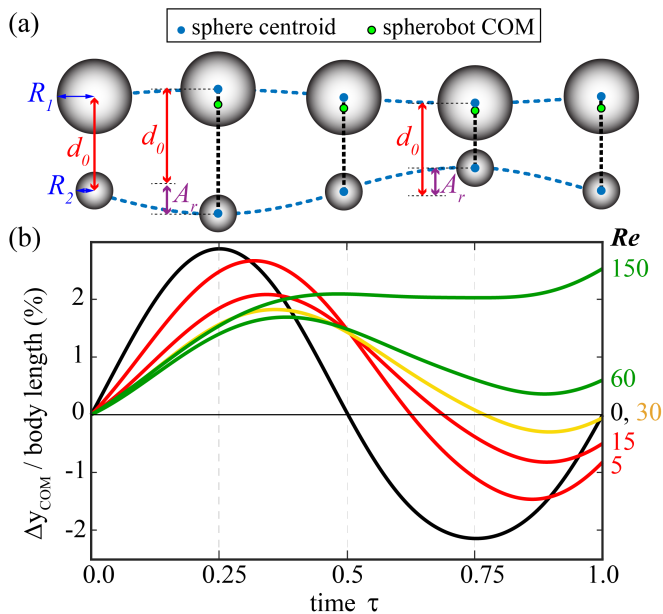
FIG. 1. (a) Reciprocal oscillation of the spherobot swimmer over one cycle. Spheres' centers of mass (COM)(blue circles) and the spherobot COM (green circle) are indicated. The distance between the spheres' centers, $d(t)$, is $d_0$, $d_0 - A_r$, and $d_0 + A_r$ at the midpoint, minimum, and maximum distances, respectively. (b) Displacement of the spherobot COM for different Reynolds numbers (0, 5, 15, 30, 60, 150) over one cycle of oscillation after steady swimming velocity. Line color indicates overall direction of swimming; swimming in the direction of the small sphere (red), large sphere (green), and no net displacement (black, yellow). Body length is $R1 + R2 + d_0 = 120$ cm.



FIG. 2. Swimming speed of the spherobot COM, $V_{\text{swim}}$, as a function of the Reynolds number. In Regime I the spherobot swims with the small sphere leading (red). At $Re \approx 30$ (yellow mark), there is a switch in direction, and in Regime II, it swims with the big sphere leading (green). The spherobot does not swim in Stokes flow, $Re = 0$ (black). Inset shows data on a logarithmic scale.

an active spring with a time-dependent equilibrium distance that was chosen to equal the prescribed distance between the spheres, $d(t)$. As a result, equal and opposite (spring) forces are applied to the spheres that act to keep them approximately at the prescribed distance apart. Because the spheres have different masses, the small sphere has a larger amplitude than the large sphere, and in our model, the ratio between the amplitudes was 8; see also Supplemental Material IC [46]. The model ensures a geometrically reciprocal cycle (error $\approx 10^{-7}$m) and a force-free swimmer. To simulate the spherobot in a fluid, we used an exactly constrained immersed boundary (CIB) method [47, 48]. The CIB scheme is implemented in the IBAMR software [49], which provides several variants of the immersed boundary (IB) method [50] for fluid-structure interaction. The IB method has been used for a variety of fluid-structure interaction problems at low [51–61], intermediate [10, 62–69], and high [49, 70–73] Reynolds numbers. Further details on our model and method are given in the Supplemental Material IA [46]. The radii of the spheres were fixed at $R_1 = 30$ cm and $R_2 = 15$ cm, and both were neutrally buoyant with respect to the surrounding fluid of density $\rho_{\text{fluid}} = 2.0$ kg-
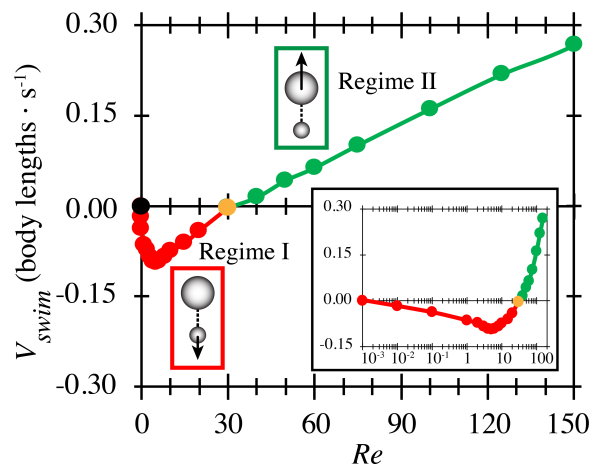
m$^{-3}$. The other parameters were fixed at $d_0 = 75$ cm, $A_r = 24$ cm, $f = 8$ Hz. $Re$ was varied from 0.001 to 150 by changing the fluid kinematic viscosity from 0.02 to 2900 $m^2s^{-1}$. The maximum ($Re = 150$) and minimum ($Re = 0.001$) were chosen so as to cover a few orders of magnitude within the intermediate range, but the specific values have no particular significance. We used the streaming Reynolds number, defined as $Re = A_r^2\omega/\nu$, which characterizes the time-averaged (steady) flow generated by oscillations at $Re_{\text{int}}$ [41, 74] and we used dimensionless time, $\tau = tf$.

**Results.** For $Re > 0$, the coupled periodic reciprocal oscillation of the two spheres resulted in the spherobot swimming (i.e., there was a net displacement of the spheres' center of mass (COM) over one cycle, $\Delta y_{\text{COM}}$) except for $Re \approx 30$. Fig. 1(a) shows a diagram of the spheres' oscillation, and Fig. 1(b) shows the corresponding COM displacements at different $Re$. Positive and negative displacements, here, are in reference to the starting position of the COM at 0. Note that the COM effectively follows the trajectory of the large, more massive sphere. For $Re = 0$, there is no net displacement over the cycle: because the cycle is reciprocal, the COM oscillates but returns to its starting position (Fig. 1(b), black curve), as required by Purcell's scallop theorem. As $Re$ increases, we see a net negative displacement over a cycle for $Re = 5, 15$ (Fig. 1(b), red curves) and a net positive displacement for $Re = 60, 150$ (Fig. 1(b), green curves). $Re = 30$ is a special point: the COM oscillates but returns to its starting position with no net displacement (Fig. 1(b), orange curve).
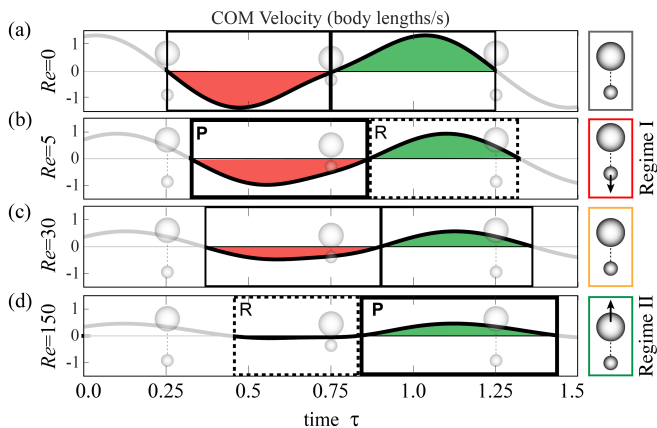
For $0.001 \leq Re \leq 150$, we calculated the spherobot

FIG. 3. The velocity of the COM of the spherobot plotted as a function of time over 1.5 cycles for (a) $Re = 0$, (b) $Re = 5$, (c) $Re = 30$, and (d) $Re = 150$. Shaded area under the curve indicates positive (green) or negative (red) displacement. Power and recovery strokes are labeled "P" and "R". Arrows on the schematic diagram on the right indicate overall direction of swimming.

swimming velocity, defined as $V_{\text{swim}} = \Delta y_{\text{COM}} f$. Plotting the velocity as a function of $Re$ (Fig. 2) allowed us to identify two regimes and two transitions: Regime I, $0.001 \leq Re < 30$, in which the spherobot swims with the small sphere at the front and the swim velocity is non-monotonic with a maximum at $Re \approx 5$ (Fig. 2, red symbols); and Regime II, $Re > 30$, in which the spherobot swims with the large sphere at the front (Fig. 2, green symbols). The regimes occurred through two transitions: (1) between $Re = 0$ and $Re = 0.001$ (our lowest non-zero $Re$ value), in which the spherobot transitions from rest to locomotion; and (2) at $Re \approx 30$, in which the spherobot switches swimming directions.

A classical approach to analyze swimmer motility is to divide the periodic motion into power and recovery strokes [2]. We defined power strokes as time intervals when the instantaneous velocity of the COM of the spherobot, $V_{\text{COM}}$, was in the mean swimming direction, and recovery strokes as time intervals when $V_{\text{COM}}$ was opposite to the mean-swimming direction. For $Re = 0$ (Fig. 3(a)), there was no distinction between power and recovery strokes, because the spherobot did not swim; instead, it moved up and down equal amounts ($V_{\text{swim}} = 0$). In Regime I (Fig. 3(b)), power and recovery strokes produce large displacements back and forth (jerky motion), resulting in a small $V_{\text{swim}}$. The back-and-forth displacements diminish with increasing $Re$ and become approximately equal at $Re \approx 30$ (areas under the curves in Fig. 3(c)). In Regime II, as $Re$ increases, the recovery stroke becomes both shorter in duration and smaller in amplitude compared to the power stroke, and compared to the recovery strokes of Regime I (Fig. 3(b)). The result is that for the higher $Re$ (e.g., $Re = 150$) in which $V_{\text{swim}}$

is large, the recovery stroke hardly exists (Fig. 3(d)), and we see less of the back-and-forth jerky motion.

To gain insight into the flow fields in each regime, we investigated instantaneous vorticity fields (Fig. 4, Supplemental Movie S1 [46]). In both regimes, there are always two vortices near the surface of each sphere. Because the flow is axisymmetric about the oscillation axis, these vortices are actually vortex rings. We shall refer to those near the sphere as inner votex rings. In Regime I (Fig 4 (a)), every time a sphere changes direction, a new inner vortex ring is generated around each sphere, pushing away the one that was there previously (now outer vortex ring) and swirling in the opposite direction (Fig. 4(a.ii)-(a.iv)). The inner vortex ring expands spatially and dominates over the outer vortex ring until the spheres change direction and the same process is repeated. Thus, for a part of the cycle, there is a single vortex ring per sphere (Fig. 4(a.iii)), and for another part of the cycle, there are two vortex rings (inner and outer) per sphere (Fig. 4(a.ii)). In Regime II (Fig 4 (b)), the vortex structures near the surface of the spheres are generated and oscillate in a similar way as in Regime I, but with one important difference: there is an additional outer vortex ring below the small sphere that does not switch direction and is never dominated by the inner vortex ring, as in Regime I. This vortex ring induces a push of fluid away from the small sphere at all times of the cycle (Fig 4 (b.i)-(b.iv), (b.vi)).

To discern the cumulative effect of the instantaneous flows in each regime, we also calculated time-averaged vorticity (Fig. 4 (v)) and velocity (Fig. 4 (vi)) fields over four cycles of oscillation. It is clear that the time-averaged flow field around the spherobot is dominated by the small sphere, *i.e.*, the magnitudes of both the vorticity and the velocity around the small sphere are higher than for the large sphere. We attribute this to the fact that the small sphere has a larger oscillation amplitude. In Regime I, the fluid, on average, pulls in towards the spheres along the direction of swimming and pushes out in the perpendicular-to-swimming direction, away from the gap between them (Fig. 4 (a.v),(a.vi)). In Regime II, the fluid, on average, does the opposite: it pushes away from the spheres along the direction of swimming (with a strong downward jet below the small sphere) and pulls in towards the gap between them in the direction perpendicular-to-swimming (Fig. 4 (b.v),(b.vi)). We thus observe that the flows around the spherobot in Regimes I and II resemble those of Stokesian pullers and pushers, respectively [23–25], even though $Re$ is in the intermediate range. (Note that the flows in all cases are symmetric about the oscillation axis).

***Discussion***. To explain our results, we invoke seminal work on steady streaming (SS), which is the nonzero time-averaged flow that arises at $Re_{\text{int}}$ because of nonlinear effects of inertia for an oscillating sphere of radius $R$ with amplitude $A$, with $A << R$ [40]. Riley's
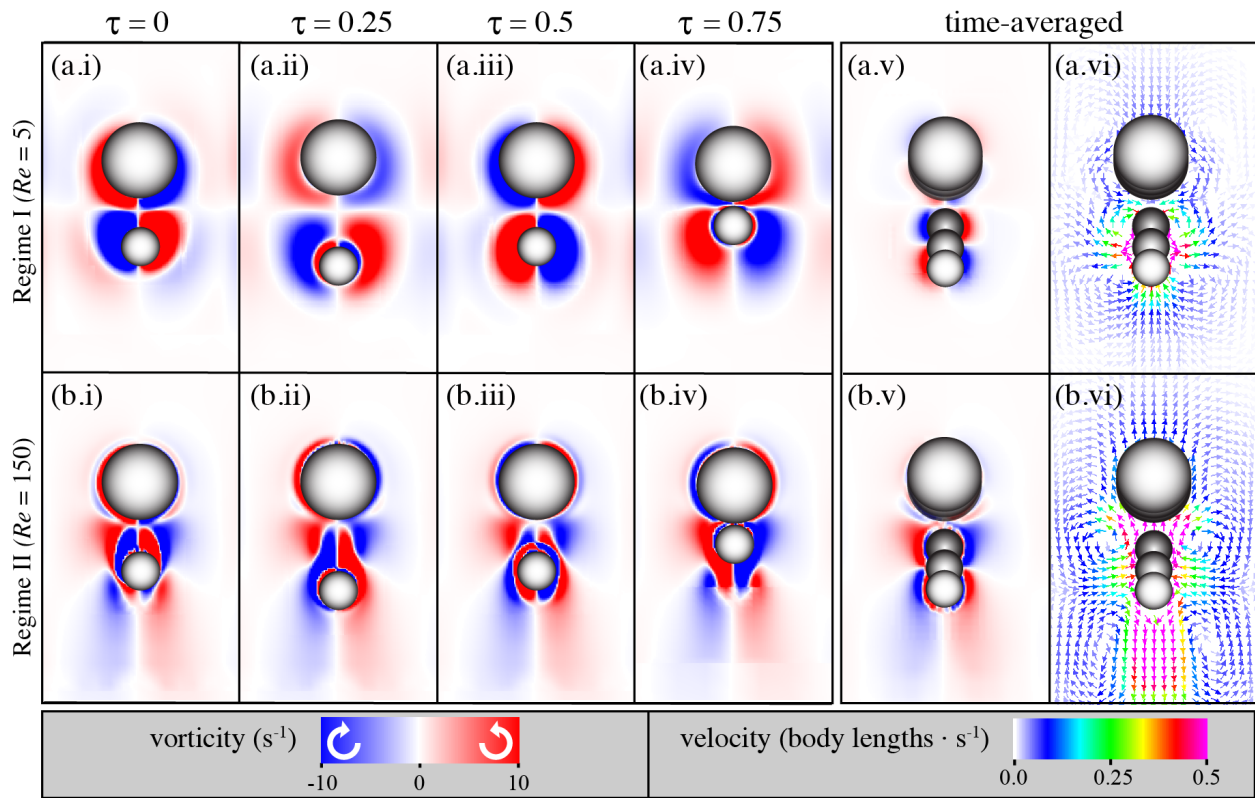
FIG. 4. Fluid flow for the two motility regimes characteristically shown for (a) $Re$=5 and (b) $Re$=150. Cross section shown is a plane through the center of the spheres (fluid flow is axisymmetric along the direction of oscillation and swimming). Instantaneous vorticity at times $\tau$ indicated at the top (i-iv); color map indicates direction and magnitude of fluid vorticity (blue for clockwise, red for counterclockwise). Time-averaged fluid (v) vorticity and (vi) velocity vector field (arrows indicate the direction of the fluid velocity vector and color indicates the magnitude). The positions of the spheres in (v–vi) indicate closest, mid-point and farthest distance during oscillation.

SS flow solutions around a sphere were calculated analytically in two cases, $R << \delta$ and $R >> \delta$, where $\delta = \sqrt{\nu/\omega}$ is the oscillatory boundary layer thickness, and were both shown to be symmetric about the oscillation axis. Even though the spherobot does not operate under the same assumptions, Riley's SS flow solutions qualitatively resemble the two flow regimes around the spherobot; see Supplemental Material III [46]. Similarly to Riley's work [40], we showed that a single oscillating sphere for $R \sim O(A)$ generates SS flow for $Re = 5$ and $Re = 150$ (corresponding to the spherobot Regimes I,II), (Fig. S5 a,b i), [75, 76].

In the case of the spherobot, the generation of SS flow by the small sphere remains practically independent of the presence of the large sphere everywhere apart from the space occupied by, or immediately adjacent to the large sphere itself, including the gap between the spheres (Fig. S5 a,b i-ii). The large sphere blocks part of the SS flow generated by the small sphere, which creates an asymmetry of the SS flows about the plane perpendicular to the oscillation axis. As a consequence of this flow asymmetry, in Regime I, the small sphere on average pulls fluid inwards along the oscillation axis so that the net flux

of momentum is towards the small sphere, causing *small-sphere-leading swimming* (Fig. 4 (a.v)). Conversely, in Regime II, the small sphere pushes fluid outwards along the oscillation axis with net flux of momentum away from the small sphere, causing it to swim in the opposite direction, i.e., *large-sphere-leading swimming* (Fig. 4 (b.v)).

We have explained why the spherobot switches swimming direction, transitioning between two motility mechanisms: an effective *steady-streaming puller* for $Re < 30$ (Regime I, Fig. 2,4a), and an effective *steady-streaming pusher* for $Re > 30$ (Regime II, Fig. 2,4b). We emphasize that our swimmer is autonomous: its SS flows are generated by its own motion rather than external stimuli [44, 77, 78] or pre-imposed flow fields, as in squirmer models [37, 38]. Further, our model is geometrically simple, reciprocal, and has essentially no *a priori* assumptions regarding its parameters, making it relatively easy to implement experimentally. For these reasons our model is a fundamental one and a step towards classification of $Re_{int}$ swimmers in general.

Many open questions remain for future investigation. For example, it would be plausible to seek connections between our model and the inertial squirmer model in

Chisholm et al. [37], in which pullers were shown to be more efficient at low nonzero $Re$ and then became unstable at higher-intermediate $Re$, while pushers became more efficient. Our swimmer in fact switches from an *SS puller* at $0 < Re < 30$ to an *SS pusher* for $Re > 30$ instead of becoming unstable, as if adapting to the surrounding fluid. Moreover, the $Re$-based transition in the observed motility mechanism will allow us to draw analogies between the spherobot and biological swimmers, which, as they grow in size and operate at higher $Re$, must change their motility mechanism. For example, the mollusk *C. antartica* switches from using cilia to flapping as it grows [79], the brine shrimp transitions from rowing to gliding with metachronally-beating legs [80], and the nymphal mayfly transitions from rowing to flapping with its gill plates [81]. Based on our findings, we suggest that steady streaming can be an important physical mechanism present more generally in motility at $Re_{\text{int}}$ both in biological organisms but also when designing artificial swimmers [42, 43, 45].

* dklotsa@email.unc.edu

[1] W. Nachtigall, Mathematical Methods in the Applied Sciences **24**, 1401 (2001).

[2] S. Vogel, *Life's devices: the physical world of animals and plants* (Princeton University Press, 1988).

[3] S. Vogel, *Life in moving fluids : the physical biology of flow* (Princeton University Press, 1994) p. 467.

[4] W. Wang, W. Duan, S. Ahmed, A. Sen, and T. E. Mallouk, Accounts of chemical research **48**, 1938 (2015).

[5] D. Patra, S. Sengupta, W. Duan, H. Zhang, R. Pavlick, and A. Sen, Nanoscale **5**, 1273 (2013).

[6] S. Tolba, R. Ammar, and S. Rajasekaran, in *Computers and Communication (ISCC), 2015 IEEE Symposium on* (IEEE, 2015) pp. 1007–1013.

[7] R. Fujiwara, T. Kano, and A. Ishiguro, Advanced Robotics **28**, 639 (2014).

[8] M. Duarte, V. Costa, J. Gomes, T. Rodrigues, F. Silva, S. M. Oliveira, and A. L. Christensen, PloS one **11**, e0151834 (2016).

[9] I. K. Bartol, P. S. Krueger, W. J. Stewart, and J. T. Thompson, The Journal of Experimental Biology (2009), 10.1242/jeb.033241.

[10] G. Herschlag and L. Miller, Journal of theoretical biology **285**, 84 (2011).

[11] S. Kern and P. Koumoutsakos, Journal of Experimental Biology **209**, 4841 (2006).

[12] L. A. Fuiman and P. W. Webb, Animal Behaviour **36**, 250 (1988).

[13] J. Sznitman, X. Shen, R. Sznitman, and P. E. Arratia, Physics of Fluids **22**, 121901 (2010).

[14] M. J. McHenry, E. Azizi, and J. A. Strother, Journal of Experimental Biology **206**, 327 (2003).

[15] A. P. S. Bhalla, B. E. Griffith, and N. A. Patankar, PLoS computational biology **9**, e1003097 (2013).

[16] J. R. Strickler, in *Swimming and flying in nature* (Springer, 1975) pp. 599–613.

[17] R. W. Blake, Canadian journal of zoology **64**, 1606 (1986).

[18] B. J. Borrell, J. A. Goldbogen, and R. Dudley, Journal of Experimental Biology **208**, 2939 (2005).

[19] B. J. Gemmell, H. Jiang, and E. J. Buskey, in *Proc. R. Soc. B*, Vol. 282 (The Royal Society, 2015) p. 20150770.

[20] H. Jiang, Journal of plankton research , fbr007 (2011).

[21] A. Najafi and R. Golestanian, Physical Review E **69**, 062901 (2004).

[22] V. B. Putz and J. Dunkel, The European Physical Journal Special Topics **187**, 135 (2010).

[23] M. Lighthill, Communications on Pure and Applied Mathematics **5**, 109 (1952).

[24] J. R. Blake, Journal of Fluid Mechanics **46**, 199208 (1971).

[25] T. J. Pedley, IMA Journal of Applied Mathematics **81**, 488 (2016).

[26] D. Saintillan and M. J. Shelley, Journal of the Royal Society, Interface / the Royal Society **9**, 571 (2012).

[27] D. Saintillan and M. J. Shelley, (2008), 10.1103/PhysRevLett.100.178103.

[28] E. Lushi and C. S. Peskin, Computers & Structures **122**, 239 (2013).

[29] L. Zhu, E. Lauga, L. Brandt, A. H. Cohen, L. J. Fauci, and R. E. Goldstein, Physics of Fluids **24**, 051902 (2012).

[30] E. Lushi, H. Wioland, and R. E. Goldstein, Proceedings of the National Academy of Sciences of the United States of America **111**, 9733 (2014).

[31] M. M. Wilhelmus and J. O. Dabiri, Physics of Fluids **26**, 101302 (2014).

[32] J. C. Nawroth and J. O. Dabiri, Physics of Fluids **26**, Art (2014).

[33] S. K. Jones, Y. J. Yun, T. L. Hedrick, B. E. Griffith, and L. A. Miller, Journal of Experimental Biology **219**, 3759 (2016).

[34] D. Krishnamurthy, G. Katsikis, A. Bhargava, and M. Prakash, Nature Physics **13**, 266 (2017).

[35] E. Lauga, Physics of Fluids **19**, 061703 (2007).

[36] S. Wang and A. Ardekani, Physics of Fluids **24**, 101902 (2012).

[37] N. G. Chisholm, D. Legendre, E. Lauga, and A. S. Khair, Journal of Fluid Mechanics **796**, 233 (2016).

[38] G. Li, A. Ostace, and A. M. Ardekani, Physical Review E **94**, 053104 (2016).

[39] E. M. Purcell, American Journal of Physics **45**, 3 (1977).

[40] N. Riley, Quart. Journ. Mech. and Applied Math **XIX**, 461 (1966).

[41] N. Riley, Annual Review of Fluid Mechanics **33**, 43 (2001).

[42] K. Ehlers and J. Koiller, (2009), arXiv:0903.3781.

[43] K. M. Ehlers and J. Koiller, Mathematical and Computer Modelling **53**, 1489 (2011), mathematical Methods and Modelling of Biophysical Phenomena.

[44] F. Nadal and E. Lauga, Physics of Fluids **26**, 082001 (2014).

[45] T. A. Spelman and E. Lauga, Journal of Engineering Mathematics **105**, 31 (2017).

[46] See Supplementary Material for more details on methods, additional figures and movies of the spherobot.

[47] B. Kallemov, A. P. S. Bhalla, B. E. Griffith, and A. Donev, Comm Appl Math Comput Sci **11**, 79 (2016).

[48] F. Balboa Usabiaga, B. Kallemov, B. Delmotte, A. P. S. Bhalla, B. E. Griffith, and A. Donev, Communications in Applied Mathematics and Computational Science **11**, 217 (2016).

[49] B. E. Griffith, R. D. Hornung, D. M. McQueen, and C. S. Peskin, Journal of Computational Physics **223**, 10 (2007).

[50] C. S. Peskin, Acta Numerica **11**, 479 (2002).

[51] S. Lim and C. S. Peskin, Physical Review E **85**, 36307 (2012).

[52] J. Teran, L. Fauci, and M. Shelley, Physical Review Letters **104**, 038101 (2010).

[53] L. J. Fauci and R. Dillon, Annu. Rev. Fluid Mech. **38**, 371 (2006).

[54] R. Dillon, L. Fauci, and D. Gaver III, Journal of theoretical biology **177**, 325 (1995).

[55] A. L. Fogelson and R. D. Guy, Computer methods in applied mechanics and engineering **197**, 2087 (2008).

[56] L. Crowl and A. L. Fogelson, Journal of fluid mechanics **676**, 348 (2011).

[57] T. G. Fai, A. Leo-Macias, D. L. Stokes, and C. S. Peskin, PLOS Computational Biology **13**, e1005790 (2017).

[58] T. G. Fai, R. Kusters, J. Harting, C. H. Rycroft, and L. Mahadevan, Phys. Rev. Fluids **2**, 113601 (2017).

[59] W. Strychalski and R. D. Guy, Biophysical journal **110**, 1168 (2016).

[60] J. Du, J. P. Keener, R. D. Guy, and A. L. Fogelson, Physical Review E **85**, 036304 (2012).

[61] S. Lim and C. S. Peskin, SIAM Journal on Scientific Computing **25**, 2066 (2004).

[62] L. A. Miller and C. S. Peskin, Journal of Experimental Biology **207**, 3073 (2004).

[63] S. Jones, R. Laurenza, T. Hedrick, B. Griffith, and L. Miller, Journal of theoretical biology **384**, 105 (2015).

[64] A. P. S. Bhalla, R. Bale, B. E. Griffith, and N. A. Patankar, J Comput Phys **250**, 446 (2013).

[65] E. D. Tytell, C.-Y. Hsu, T. L. Williams, A. H. Cohen, and L. J. Fauci, Proceedings of the National Academy of Sciences **107**, 19832 (2010).

[66] E. D. Tytell, M. C. Leftwich, C.-Y. Hsu, B. E. Griffith, A. H. Cohen, A. J. Smits, C. Hamlet, and L. J. Fauci, Physical Review Fluids **1**, 073202 (2016).

[67] A. P. Hoover, B. E. Griffith, and L. A. Miller, Journal of Fluid Mechanics **813**, 1112 (2017).

[68] W. Kou, B. E. Griffith, J. E. Pandolfino, P. J. Kahrilas, and N. A. Patankar, Journal of computational physics **348**, 433 (2017).

[69] W. Kou, A. P. S. Bhalla, B. E. Griffith, J. E. Pandolfino, P. J. Kahrilas, and N. A. Patankar, Journal of computational physics **298**, 446 (2015).

[70] B. E. Griffith, International Journal for Numerical Methods in Biomedical Engineering **28**, 317 (2012).

[71] A. Hasan, E. M. Kolahdouz, A. Enquobahrie, T. G. Caranasos, J. P. Vavalle, and B. E. Griffith, Medical Engineering and Physics **47**, 72 (2017).

[72] V. Flamini, A. DeAnda, and B. E. Griffith, Theoretical and computational fluid dynamics **30**, 139 (2016).

[73] H. Gao, L. Feng, N. Qi, C. Berry, B. E. Griffith, and X. Luo, Medical Engineering and Physics **47**, 128 (2017).

[74] F. Otto, E. K. Riegler, and G. A. Voth, Physics of fluids **20**, 093304 (2008).

[75] D. Klotsa, M. R. Swift, R. M. Bowley, and P. J. King, Phys. Rev. E **76**, 056314 (2007).

[76] D. Klotsa, M. R. Swift, R. M. Bowley, and P. J. King, Phys. Rev. E **79**, 021302 (2009).

[77] H. S. Wright, M. R. Swift, and P. J. King, Phys. Rev. E **78**, 036311 (2008).

[78] D. Klotsa, K. A. Baldwin, R. J. Hill, R. M. Bowley, and M. R. Swift, Physical review letters **115**, 248102 (2015).

[79] S. Childress and R. Dudley, Journal of Fluid Mechanics **498**, 257 (2004).

[80] T. A. Williams, The Biological Bulletin **187**, 164 (1994).

[81] A. T. Sensenig, K. T. Kiger, and J. W. Shultz, Biological journal of the Linnean Society **98**, 540 (2009).